ACS APPLIED MATERIALS & INTERFACES

www.acsami.org Research Article

Tailoring Multiple Sites of Metal–Organic Frameworks for Highly Efficient and Reversible Ammonia Adsorption

Zhenzhen Wang, Zhiyong Li,* Xia-Guang Zhang, Qingchun Xia, Huiyong Wang, Chenlu Wang, Yanlei Wang, Hongyan He, Yang Zhao, and Jianji Wang*

Cite This: *ACS Appl. Mater. Interfaces* 2021, 13, 56025–56034 Read Online

ACCESS | Metrics & More | Article Recommendations | Supporting Information

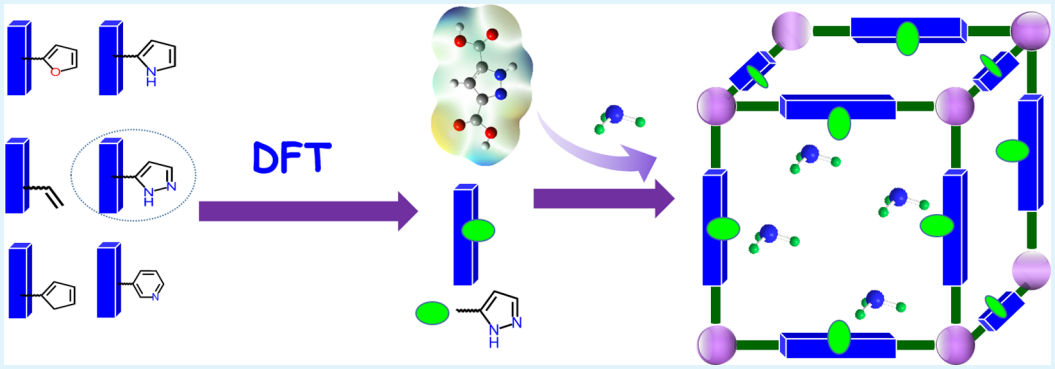

ABSTRACT: The structural diversity and designability of metal–organic frameworks (MOFs) make these porous materials a strong candidate for NH_3 uptake. However, to achieve a high NH_3 capture capacity and good recyclability of MOFs at the same time remains a great challenge. Here, a multiple-site ligand screening strategy of MOFs is proposed for highly efficient and reversible NH_3 uptake for the first time. Based on the optimized DFT results for various possible ligands, pyrazole-3,5-dicarboxylate with multiple sites was screened as the best ligand to construct robust MOF-303(Al) with Al^{3+}. It is experimentally found that the NH_3 adsorption capacity of MOF-303(Al) is as high as 19.7 mmol g^{-1} at 25.0 °C and 1.0 bar, and the NH_3 capture is fully reversible and no clear loss of capture capacity is observed after 20 cycles of adsorption–desorption. Various spectral studies verify that the superior NH_3 capacity and excellent recyclability of MOF-303(Al) are mainly attributed to the hydrogen bonding interactions of NH_3 with multiple sites of MOF-303(Al).

KEYWORDS: *ammonia, metal–organic framework, high and reversible capture, multiple-site interactions, hydrogen bonding*

INTRODUCTION

Ammonia (NH_3) is one of the most important chemicals in the world and is widely used in many commercial applications.[1−4] Meanwhile, NH_3 is also a typical basic, colorless, corrosive, and toxic gaseous pollutant and a key factor for the formation of particulate matter 2.5 (PM2.5).[5,6] The emission of NH_3 into the atmosphere is greatly harmful to the environment and human health. Therefore, the capture and recovery of gaseous NH_3 from various industries are highly desirable for both environmental protection and resource utilization.[7] A variety of materials such as activated carbons, zeolites, mesoporous silica, and organic polymers have been used for the capture of NH_3,[8−13] but most of them show a low adsorption capacity, and the recovery of NH_3 is also a big problem.

Metal–organic frameworks (MOFs) have shown great potential in gas adsorption and storage[14−17] due to their large specific surface area, high pore volume, tunable chemical structure, and Lewis acidic metal sites.[18−22] Theoretically, MOFs with various structures and functions can be obtained through the design of ligands and metal nodes. This feature of MOFs provides the possibility for their application in ammonia capture and storage. However, as far as NH_3 adsorption is concerned,[23−34] the framework collapse of MOFs is often reported because of the strong coordination of NH_3 to the metals on the frameworks. For example, structural collapse was observed during adsorption of NH_3 by typical MOF materials such as MOF-5, MOF-177, Cu-MOF-74, and Cu_3BTC_2,[23−25] owing to the strong interactions between NH_3 and the metal Zn/Cu sites. Even for stable Zr-based MOFs, the frameworks could not be maintained after adsorption of NH_3.[26,35] On the other hand, using the ligands with stronger donating ability for

Received: July 30, 2021
Accepted: November 8, 2021
Published: November 17, 2021

https://doi.org/10.1021/acsami.1c14470
ACS Appl. Mater. Interfaces 2021, 13, 56025–56034

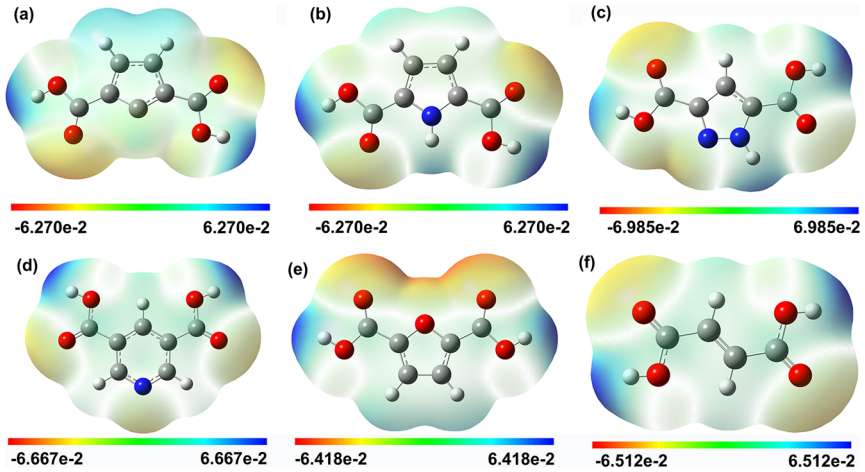

Figure 1. Electrostatic potential maps for the ligands (a) 3,5-cyclopentadiene-1,3-dicarboxylic acid (CP), (b) 2,5-pyrroldicarboxylic acid (PC), (c) pyrazole-3,5-dicarboxylate (PDC), (d) 3,5-pyridinedicarboxylic acid (PYDC), (e) 2,5-furandicarboxylic acid (Fur), and (f) fumaric acid (Fum); red, O atom; blue, N atom; gray, C atom; white, H atom.

the metals, such as pyrazolate,[14] could improve the tolerance of the frameworks to NH_3 to a certain extent.[26,27] In this case, the uptake capacity of NH_3 was reported to be 19.79 mmol g^{-1} at 25.0 °C and 1.0 bar,[26] but the partial collapse of the framework is still unavoidable. This problem leads to the difficulty in the cyclic utilization of MOFs and seriously hinders the practical application of MOFs in NH_3 capture and recovery.

Therefore, for efficient and reversible absorption of NH_3, MOFs are required to have inert metals to NH_3; in this way, stable MOFs under a NH_3 atmosphere and good cycle performance may be achieved. In this regard, to choose weakly coordinated metals with NH_3 and strongly interacting ligands with metals is a good strategy since the strong interactions between ligands and metals may reduce the coordination of metals with NH_3. For example, MFM-300 (Al, Fe, V^{III}, and Cr), MIL-53, MIL-100, and MIL-101,[30,36,37] constructed by inert metals and carboxylate ligands, are stable to the exposure of NH_3. Among these MOFs, MFM-300(Al) shows reversible uptake of NH_3 over 50 cycles without losing its crystallinity.[30] These results are promising for reversible NH_3 adsorption, but the adsorption capacity is not high due to the lack of contribution from metal sites. Recently, it is reported that robust Mg_2(dobpdc) with an open Mg^{2+} site creates the record value of 23.9 mmol g^{-1} for the uptake of NH_3.[38] Interestingly, it is stable for NH_3 due to the stronger affinity of Mg^{2+} for oxygen atoms in the ligands than the nitrogen atom of NH_3. Nevertheless, because of the stronger interactions between Mg^{2+} and NH_3, the desorption peak temperature for Mg_2(dobpdc) was 249 °C under vacuum, indicating that the recycle performance should be improved. Therefore, to achieve a high adsorption capacity of NH_3 and good recyclability of MOFs at the same time is a significant challenge.

To address these problems, in this work, a multiple-site ligand screening strategy of MOFs is proposed for highly efficient and reversible NH_3 uptake for the first time. Considering the fact that Al^{3+} is relatively inert toward NH_3, Al^{3+} was used in the construction of MOFs. Instead of using relative active metals such as Mg^{2+} mentioned above to increase the NH_3 capacity, we hope to achieve a high NH_3 capacity by increasing the number of active sites in the ligands. In this way, desorption of NH_3 and recycling of the MOFs would be easier because interaction of any physical site of the ligands with NH_3 is weaker than that of active metals with NH_3. Here, the ligand with a carboxyl group is designed as the basic structural unit of MOF because it can form robust MOFs with Al^{3+}.[30,37] Inspired by the fact that introducing polar functional groups into the ligands of MOFs is an effective strategy to increase the capture capacity of gas, such as CO_2[39−41] and NH_3,[31] this strategy is adopted to construct MOFs with a high ammonia capacity. On the other hand, to avoid using an empirical trial-and-error method for searching optimal ligands, a simple and efficient density functional theory (DFT) approach is used for the molecular design of the ligands before experimental attempts. As a result of theoretical calculations, pyrazole-3,5-dicarboxylate (PDC) with multiple sites was screened from six kinds of possible ligands (see the chemical structure in Figure S1) as the "best" ligand for constructing robust MOF-303(Al). Then, the interaction energy and structure parameters of the adsorption configuration between MOF-303(Al) and NH_3 were calculated, and strong multiple hydrogen interactions were observed between MOF-303(Al) and NH_3. Under the guidance of these theoretical results, MOF-303(Al) was experimentally synthesized and used for NH_3 uptake at 25.0 °C and 1.0 bar. Interestingly, a high adsorption capacity (19.7 mmol g^{-1}) and fully reversible recycling (at least 20 cycles) at 150 °C were indeed achieved simultaneously. Combined spectral results verified that the superior NH_3 capacity and excellent recyclability are mainly attributed to the multiple hydrogen bonding interactions of NH_3 with sites of MOF-303(Al), which is in accordance with our theoretical predictions.

RESULTS AND DISCUSSION

Ligand Screening of MOFs. Molecular electrostatic potential (MEP) is a simple but important descriptor to study interactions, including coordination, electrostatic, and hydrogen bonding in chemical systems.[42,43] To optimize ligands with promising adsorption sites for NH_3, MEP values were calculated for six kinds of possible ligands (see details in the Supporting Information), and the results are illustrated in Figure 1. These values are defined by different colors on the surface; from red to blue, the potential is increased. Clearly, the N and O atoms have negative electrostatic potential, and they could interact with the H atom of NH_3, while C and H atoms

https://doi.org/10.1021/acsami.1c14470
ACS Appl. Mater. Interfaces 2021, 13, 56025−56034

have positive electrostatic potential, and an opposite function would be predicted. To quantify the charge carried by the atoms, the charge of each atom of the ligands was calculated by DFT (Figure S2). Compared to the other ligands, PDC has two negatively charged N atoms, and the N−N site may interact with the H atom in NH_3 molecules. At the same time, the H atom on the H−N group of PDC has a significant positive charge ($0.427e^-$), which could form a hydrogen bond with the N atom of NH_3. The charge of H on the C−H group of PDC is $0.254e^-$, indicating that the C−H site may be another potential adsorption site for NH_3. Furthermore, the N−N and N−H sites may synergistically adsorb multiple NH_3 molecules. Therefore, PDC may be an excellent MOF ligand for NH_3 capture.

Based on the above results, PDC was considered as the optimal ligand to construct MOF-303(Al) with Al^{3+}; the framework structure is shown in Figure S3a, and the extended structure of the calculated MOF-303(Al) is given in Figure S3b. The interaction energies of NH_3 with each of the possible adsorption sites on MOF-303(Al) and the structure parameters of the hydrogen bonds between NH_3 and the MOF were calculated by DFT (see details in the Supporting Information), and the results are given in Figure S4 and Table 1. It is clear that N−H and μ-OH (it is created between the Al atoms on the framework in the formation of MOF-303(Al)) have high hydrogen bonding interaction energies of −0.72 and −0.51 eV with NH_3, and the hydrogen bond lengths of N−H(MOF)···N(NH_3) and O−H(MOF)···N(NH_3) were 1.74 and 1.98 Å, respectively. These results indicate that strong hydrogen bonds were formed between MOF-303(Al) and NH_3,[44] and the possible contribution of the H−N site to the NH_3 adsorption capacity is much higher than that of the μ-OH site. On the other hand, hydrogen bonding interaction energies between NH_3 and C−H site or N−N site of PDC were −0.27 and −0.29 eV, respectively, suggesting that similar weak hydrogen bonds (C−H(MOF)···N(NH_3) and N−N(MOF)···H(NH_3)) were formed. These results suggest the presence of multiple and strong hydrogen bonding interactions between MOF-303(Al) and NH_3, and this MOF is expected to be useful for high-efficiency capture of NH_3.

Table 1. Hydrogen Bonding Interaction Energy (HBIE) and Hydrogen Bond Length (HBL) of NH_3 Adsorption on MOF-303(Al)

site	HBIE/eV	type of hydrogen bond	HBL/Å
H−N	−0.72	N−H(MOF)···N(NH_3)	1.74
H−O[a]	−0.51	O−H(MOF)···N(NH_3)	1.98
N−N	−0.29	N−N(MOF)···H(NH_3)	2.30
H−C	−0.27	C−H(MOF)···N(NH_3)	2.31

[a]H−O is the μ-OH site in the MOF.

NH_3 Adsorption Performance of MOF-303(Al). Under the guidance of these theoretical results, MOF-303(Al) was synthesized by a solvothermal approach using the procedures reported in the literature[45] and then characterized by powder X-ray diffraction (PXRD), thermogravimetric analysis (TGA), and N_2 adsorption isotherms, and the results are presented in Figure 2. It was shown that the PXRD patterns (Figure 2a) of the as-synthesized MOF are in good agreement with that of MOF-303(Al) reported in the literature.[45] The permanent porosity of MOF-303(Al) was confirmed by N_2 adsorption measurements at 77 K (Figure 2b). This material exhibits the type I isotherm, indicating its microporous character. As shown in Table S1, the pore size for MOF-303(Al) is 0.59 nm, which was larger than that of NH_3 (0.3 nm).[20] The high BET surface area (1292 m^2/g) and suitable pore size make it possible for MOF-303(Al) to be used for NH_3 adsorption. The TGA data reveal that the frameworks of MOF-303(Al) start to decompose at around 400 °C under a N_2 atmosphere (Figure 2c), demonstrating the excellent thermal stability. The mass loss from 20 °C to 100 °C is likely due to the loss of any residual solvents from the pores.[46] Moreover, the chemical stability of MOF-303(Al) was investigated by soaking it in

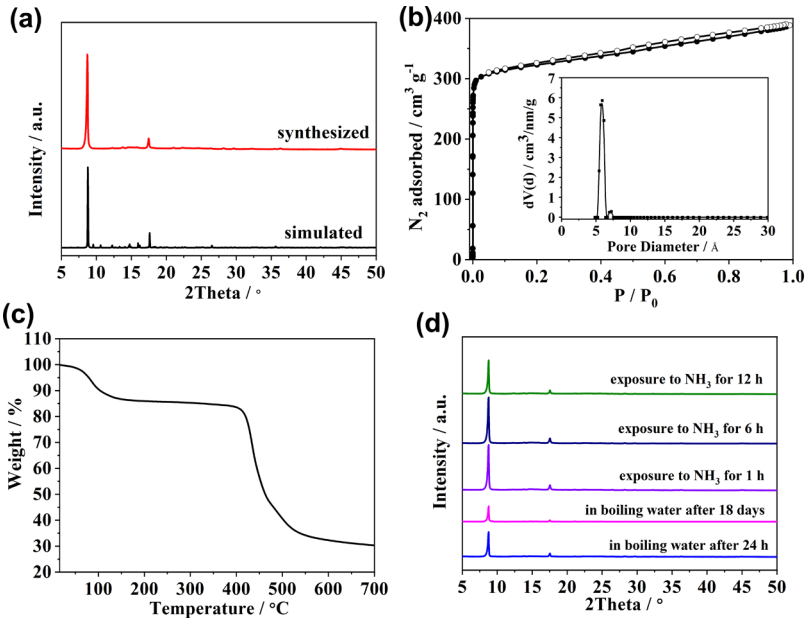

Figure 2. (a) PXRD patterns of MOF-303(Al); (b) N_2 adsorption isotherms and DFT pore size distribution of MOF-303(Al) at 77 K; (c) TGA curves of MOF-303(Al) under a N_2 atmosphere; (d) PXRD patterns of MOF-303(Al) before and after exposure to NH_3 or boiling water for a different time.

https://doi.org/10.1021/acsami.1c14470
ACS Appl. Mater. Interfaces 2021, 13, 56025−56034

boiling water for 18 days or exposing it to NH_3 up to 12 h. As illustrated by PXRD patterns (Figure 2d), the crystallinity of MOF-303(Al) was completely retained after these treatments.

To assess the NH_3 adsorption performance of MOF-303(Al), the adsorption isotherm of NH_3 was determined at 25.0 °C and 1.0 bar, and the adsorption capacity was found to be 19.7 ± 0.2 mmol g^{-1} (Figure 3a). This is close to the record

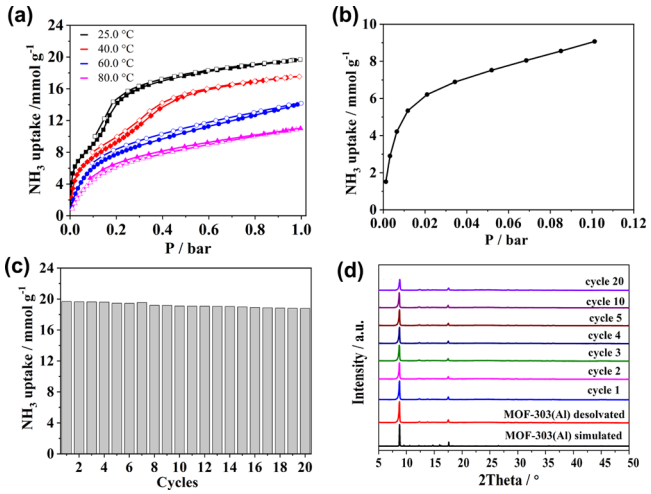

Figure 3. (a) NH_3 adsorption isotherms on MOF-303(Al) at different temperatures; (b) adsorption curve of NH_3 on MOF-303(Al) at a low pressure; (c) NH_3 uptake of MOF-303(Al) over 20 cycles; NH_3 was absorbed at 25.0 °C, while the MOF was regenerated at 150 °C under vacuum; (d) PXRD patterns of MOF-303(Al) before and after recycling.

value reported recently.[38] The reliability of our experimental instrument was confirmed by measurement of the NH_3 adsorption capacity of MIL-101(Cr) MOF (see Methods), which has been reported in the literature.[36] The sharp increase step at a low pressure area was attributed to NH_3 adsorption preferentially by the μ-OH or −NH group in the framework through hydrogen bonding interactions.[37] Moreover, MOF-303(Al) exhibited a great packing density of NH_3 at 0.61 g cm^{-3}, which is higher than most of the state-of-the-art porous materials (Table S2),[26,30,47] indicating that MOF-303(Al) could be used for the high density storage of NH_3 for energy application. Furthermore, the NH_3 adsorption capacity of MOF-303(Al) at 80.0 °C was 11.0 ± 0.2 mmol g^{-1} (Figure 3a), showing that there was a strong interaction between NH_3 and MOF-303(Al) at higher temperatures. This is an exciting result, because it provides the possibility for the direct adsorption of NH_3 from industrial waste gas without cooling.[48] The small step of the ammonia adsorption isotherms at 25.0 and 40.0 °C was attributed to the strong hydrogen bonding interactions of NH_3 with μ-OH and −NH sites in the framework, which results in the condensation of NH_3 in the pore of MOF-303(Al). The hydrogen bonding interactions decreased with the increase in temperature; therefore, the NH_3 condensation disappeared at 60.0 and 80.0 °C, and the typical type I profile was observed.

In addition, the CO_2 adsorption capacity of MOF-303(Al) was found to be 1.44 mmol/g at 80.0 °C (Figure S5), and the theoretical selectivity adsorption coefficient was 7.6 for NH_3/CO_2. This result suggests that MOF-303(Al) also shows potential for selective separation of NH_3 over CO_2 from waste gas of some industries (such as production of melamine) at higher temperatures, which is very difficult when the reported adsorbents are used. The CO_2 adsorption isotherm of MOF-303(Al) at 80.0 °C shows a linear adsorption (Figure S5), which seems to deviate from standard IUPAC adsorption isotherm types.[49] Here, it should be emphasized that the standard IUPAC adsorption isotherm types were determined under a critical temperature of the adsorptive (0 °C for CO_2). To clarify this point, we determined CO_2 adsorption isotherms on MOF-303(Al) at different temperatures. It is shown that a type I isotherm was really obtained at 0 °C (Figure S5), and the curves gradually become linear as the temperature increases. Therefore, the linear CO_2 adsorption isotherm observed here is attributed to the high experimental temperature.

Furthermore, the adsorption capacity at the lowest-pressure point on the desorption curve of MOF-303(Al) was found to be 10.0 mmol g^{-1} (Figure 3a), corresponding to 1.98 molecules of NH_3 per framework unit. This suggests that each framework unit of MOF-303(Al) strongly binds two molecules of NH_3 to form a very stable MOF-303(Al)-NH_3 complex. Combination of HBIE and HBL data in Table 1 indicates that H−N and μ-OH sites had a major contribution to ammonia absorption of MOF-303(Al), especially at a low pressure area. Surprisingly, the NH_3 uptake capacity at 0.01 bar was up to 5 mmol g^{-1} (Figure 3b). This result indicates that MOF-303(Al) has excellent NH_3 adsorption ability at extremely low concentrations and could be used for the trace ammonia contaminant removal from polluted air due to the unique pore environment decorated with active μ-OH and −NH sites in MOF-303(Al).[34]

Then, the reversibility of NH_3 adsorption by MOF-303(Al) was evaluated. It is interesting to note that the absorbed NH_3 could be removed at 150 °C under vacuum for 2 h. The highly efficient uptake and desorption were reversible over 20 cycles (Figure S6) with only 5% loss in capacity (Figure 3c). In addition, the activated MOF-303(Al) did not lose crystallinity and change morphology, as confirmed by the PXRD patterns and scanning electron microscopy (SEM) images of the MOFs before and after NH_3 adsorption (Figure 3d and Figure S7). As shown in Figure S8 and Table S1, the lower BET surface area (848 m^2 g^{-1}) was also determined for MOF-303(Al) after NH_3 adsorption. However, the clear loss of porosity for MOF-303(Al) did not induce a decline in NH_3 uptake capacity during recycling. This result suggests that although the BET area decreases, the adsorption sites that bind NH_3 strongly still remain accessible. Therefore, previous observations reported in the literature[11,27,50] indicate that a decrease in BET area is not predictive of a decline in NH_3 uptake that was confirmed.[11,27,51] Careful analysis of PXRD patterns indicates that the lower angle peak of MOF-303(Al) broadens and decreases in intensity in the adsorption and desorption cycle (Figure S9), which is indicative of a slight disorder that happened in the structure of MOF-303(Al), leading to a slight decrease in BET area and total adsorption capacity.[52] To evaluate the regeneration performance of MOF-303(Al) used in this work, the regeneration conditions of typical porous materials that absorb ammonia, together with their NH_3 capacity, are summarized in Table S3 in the Supporting Information. It was shown that the regeneration temperature of the materials was mild when the ammonia capture capacity was relatively low. However, the regeneration of porous materials with a high ammonia capacity usually requires a higher temperature and longer time under vacuum. For example,

https://doi.org/10.1021/acsami.1c14470
ACS Appl. Mater. Interfaces 2021, 13, 56025−56034

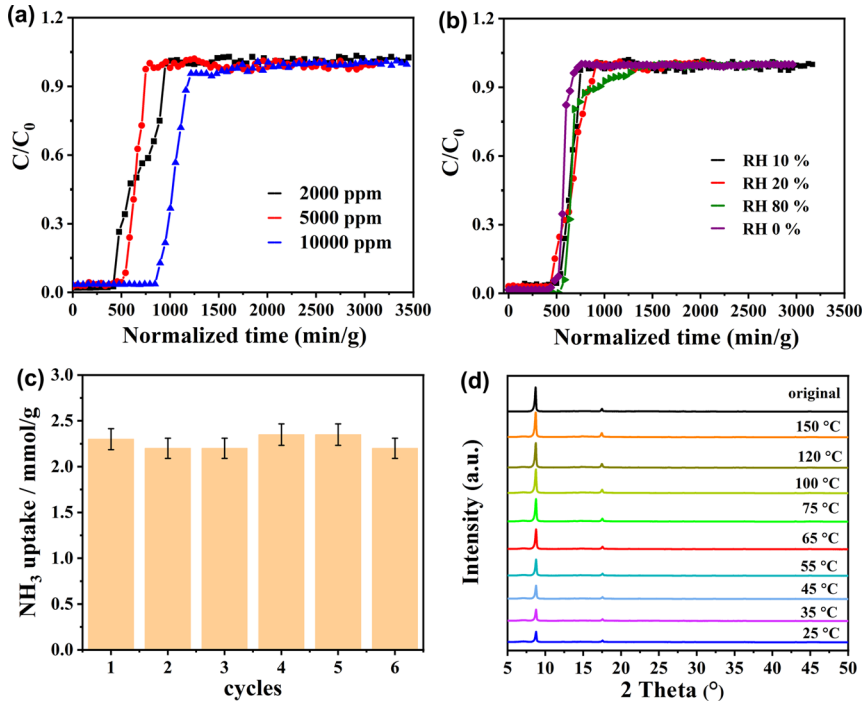

Figure 4. (a) NH_3 absorption capacity of MOF-303(Al) for the NH_3/N_2 mixtures containing 2000, 5000, and 10,000 ppm of ammonia at 10% RH; (b) NH_3 absorption capacity of MOF-303(Al) for the NH_3/N_2 mixture containing 5000 ppm of ammonia as a function of RH; (c) NH_3 breakthrough capacity of MOF-303(Al) at 5000 ppm of NH_3 and 10% RH for different cycles; (d) variable temperature PXRD patterns of MOF-303 (Al) after humid NH_3 adsorption.

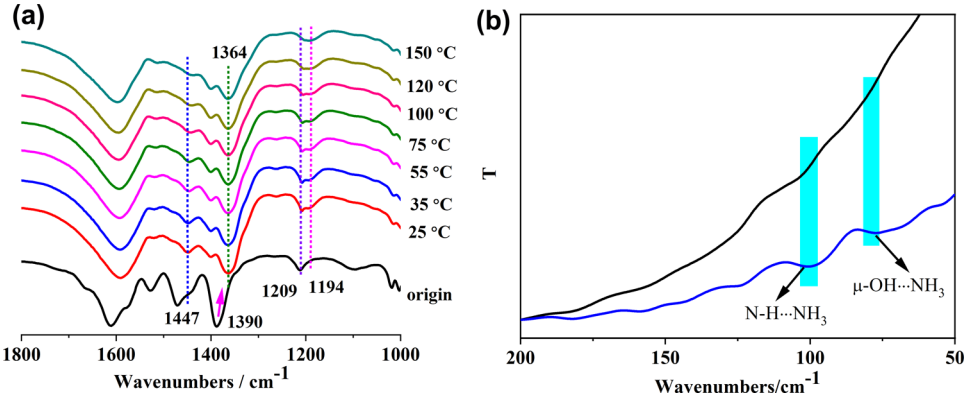

Figure 5. (a) Enlarged mid-IR spectra of MOF-303(Al) after NH_3 adsorption at different temperatures and normal pressure; (b) far-infrared spectra of MOF-303(Al) before (black line) and after (blue line) NH_3 adsorption.

UiO-66-NH_2 could adsorb 9.8 mmol/g NH_3 and then be regenerated at 150 °C for 12 h under vacuum.[27] Considering the high capture capacity of ammonia by MOF-303(Al), the regeneration condition (150 °C under vacuum for 2 h) is advantageous. This result indicates that our philosophy to prepare an MOF with an efficient and reversible NH_3 capacity is effective.

Humid NH_3 Adsorption Performance of MOF-303(Al). To investigate the actual application of MOF-303(Al) for the capture of a small amount of NH_3 in air, breakthrough experiments of NH_3/N_2 mixtures containing different contents of ammonia (2000, 5000, and 10,000 ppm) were performed at 25.0 °C as a function of relative humidity (RH), and the results are exhibited in Figure 4a,b. It can be seen that the NH_3 absorption capacities were 0.8, 2.3, and 4.2 mmol/g for the gas mixtures containing 2000, 5000, and 10,000 ppm of ammonia at 10% RH, respectively. For the given content of ammonia at 5000 ppm, the NH_3 absorption capacities at 0% (dry gas), 10%, 20%, and 80% RH were 2.2, 2.3, 2.3, and 2.8 mmol/g, respectively. These results indicate that MOF-303(Al) could capture a low content of ammonia in a wide range of humidity, and a few effects might be found in the ammonia capture capacity of MOF-303(Al) in the presence of moisture. To evaluate the capture capacity of MOF-303(Al) for humid NH_3, the capacities of MOF-303(Al) and typical porous materials at different RH values and NH_3 contents are listed in Table S4. It was shown that the adsorption capacity of MOF-303(Al) for ammonia was at a medium level under certain humidity conditions. The possible reason is that MOF-303(Al) lacked the important contribution of metals to ammonia adsorption to avoid the collapse of the framework.

Moreover, the reversibility of NH_3 adsorption by MOF-303(Al) in the presence of moisture was evaluated. It is interesting to find from Figure 4c and Figure S10 that the NH_3

https://doi.org/10.1021/acsami.1c14470
ACS Appl. Mater. Interfaces 2021, 13, 56025−56034

uptake and desorption at low ammonia contents were reversible under 10% RH for at least six cycles with no clear loss in capacity. Then, the variable temperature PXRD of MOF-303(Al) after humid NH_3 adsorption was determined to examine the stability of the MOF, and the results are given in Figure 4d. It can be seen that the PXRD pattern of MOF-303(Al) decreased in intensity obviously at 25.0 °C after humid NH_3 adsorption. On the other hand, the intensity of PXRD patterns gradually increased with the increase in temperature. When the temperature reached 100 °C, the intensity was generally consistent with that of the original MOF-303(Al). Furthermore, no position change of the diffraction peaks was observed at this temperature, indicating that MOF-303(Al) was stable after humid NH_3 adsorption. The result for the decrease in diffraction peak intensity at a lower temperature could be explained by the coexistence of water and ammonia in the pore of MOF-303(Al).

Mechanism of NH_3 Adsorption by MOF-303(Al). Far-IR spectroscopy, variable temperature mid-IR spectroscopy, and X-ray photoelectron spectroscopy (XPS) were used to verify the interactions between NH_3 and MOF-303(Al). From the variable temperature mid-IR spectra shown in Figure S11, several features were observed, and these are partly exhibited in Figure 5a. Notably, after NH_3 adsorption, the peak at 1209 cm^{-1} for the original MOF-303(Al) was red-shifted with a slightly decreased trend as the temperature was increased, and a new peak appeared at 1194 cm^{-1}. Based on our calculated IR spectra (Figure S12) and previous investigations reported in the literature,[53] the peak at 1209 cm^{-1} could be attributed to the N−H in-plane rocking of PDC of the MOF. The red shift of this peak indicated strong hydrogen bonding interaction between NH_3 and the N−H site of the MOF after NH_3 adsorption. The new peak at 1194 cm^{-1} was assigned to the bending of three N−H groups of the adsorbed NH_3 on the N−H site of the MOF. In addition, in the vibration region of 750−500 cm^{-1}, the peak at 660 cm^{-1} attributed to the bending of μ-OH disappeared (Figure S11) due to its hydrogen bonding interaction with NH_3.

The hydrogen bonding interactions between NH_3 and MOF-303(Al) could also be understood from the other mid-IR peaks. As shown in Figure 5a, the strength enhancement in the N−N stretching of pyrazole ring at 1447 cm^{-1} was attributed to the deformation vibration of pyrazole ring caused by the hydrogen bonding interactions of NH_3 with N−N and N−H sites.[53,54] With increasing temperature to 150 °C, desorption of NH_3 led to the reversion of the band position shift. At the same time, the symmetrical stretching vibration of $-COO^-$ at 1390 cm^{-1} disappeared and the characteristic symmetric deformation of NH_3 was observed at 1364 cm^{-1} after NH_3 adsorption,[55,56] and its peak intensity decreased with the increase in temperature. This originated from the interaction between the Al−O cluster of MOF-303(Al) and NH_3 (Figure S13). In addition, broad peaks between 2600 and 4000 cm^{-1} are another feature of Figure S11. We fitted these peaks with a Win-IR curve-fitting procedure and found that the components that contributed to the broad peaks are complicated, and the high adsorption of the C−H group in this area makes the spectral analysis more complicated. However, the contribution of the interaction between μ-OH and NH_3 was clearly observed (Figure S14). The stronger antisymmetric stretching vibration at 3414 cm^{-1} and the symmetric stretching vibration at 3336 cm^{-1} of NH_3[57] indicate again strong NH_3 adsorption by MOF-303(Al) (Figures S11 and S14). The stretching vibration of μ-OH at 3641 cm^{-1} shifted to 3578 cm^{-1} after NH_3 adsorption, demonstrating the strong hydrogen bonding interaction of μ-OH with NH_3.[30] Moreover, the characteristic peaks of NH_3 did not disappear after heating up to 150 °C under normal pressure, which suggests the strong hydrogen bonding interactions between MOF-303(Al) and NH_3 once again. These results reveal that the multiple-site (N−H, μ-OH, H−C, and N−N) hydrogen bonding interactions between MOF-303(Al) and NH_3 are responsible for the highly efficient adsorption and desorption of NH_3.

Far-IR spectroscopy, which is known as a powerful tool for the characterization of hydrogen bonding in gas and condensed states,[58] was used to verify the formation of hydrogen bonds between NH_3 and MOF-303(Al). As shown in Figure 5b, two new peaks were observed at 100 and 77 cm^{-1}, which could be assigned to the stretching vibration of hydrogen bonds between the N atom in NH_3 and the H atom in both N−H and μ-OH sites of MOF-303(Al) (Figure S15). Moreover, the experimental values of the vibrational peaks are in line with the calculated ones from DFT (Figure S16). However, the weaker hydrogen bonding interactions of NH_3 with the N−N and C−H sites were not detected after NH_3 adsorption. These results indicate that hydrogen bonds were formed between NH_3 and MOF-303(Al) and the strong hydrogen bonding interaction of NH_3 with the N−H and μ-OH sites of MOF-303(Al) was the main driving force for the high NH_3 capture capacity. We try to use the variable temperature far-IR spectra of MOF-303(Al) after NH_3 adsorption to see the gradual evolution of the peaks at 77 and 100 cm^{-1} in the temperature range from 25 to 100 °C that originated from the dominant H-bonding interactions. However, we did not obtain satisfactory results because of the weak signal of the far-infrared spectrum.

To further prove the hydrogen bonding interactions between NH_3 and MOF-303(Al), the XPS spectra of MOF-303(Al) were determined before and after NH_3 adsorption. It can be seen from Figure S17 that N 1*s* photoemission in MOF-303(Al) occurred at 400.0 eV before NH_3 adsorption and increased to 400.2 eV after NH_3 adsorption due to the formation of strong hydrogen bonds between NH_3 and MOF-303(Al).[59] However, because of the weak signal of NH_3, its N 1*s* binding energy at 397.9 eV could not be isolated.[60] Moreover, Al 2*p* photoemission in MOF-303(Al) decreased from 74.5 eV to 74.2 eV after NH_3 adsorption, indicating the change in electron cloud density around Al. The possible reason for this result is the adsorption of NH_3 on the Al−O cluster of MOF-303(Al) (Figure S13), which affects the binding energy of Al 2*p*. It should be noted that this is a weak interaction and may not obviously affect the stability of the framework of MOF-303(Al). Therefore, the contribution of the metal Al site to the NH_3 absorption capacity is relatively low. Contrary to expectations, the binding energies of O 1*s* did not show any significant change after NH_3 adsorption (Figure S18).

To compare the effect of the number of absorption sites on the NH_3 capacity, three other MOFs with different ligands, including MIL-160, CAU-10-pydc, and Al-Fum, were also prepared by using the procedures reported in the literature.[46,52,61] For these MOFs, MIL-160 has two sites (O−C and μ-OH sites), and CAU-10-pydc also has two sites (N−C and μ-OH sites), while Al-Fum only has a μ-OH site (see the framework structure in Figure S19). Then, these MOFs were characterized by PXRD, TGA, and N_2 adsorption isotherms,

https://doi.org/10.1021/acsami.1c14470
ACS Appl. Mater. Interfaces 2021, 13, 56025−56034

and the results (Figures S20−S23 and Table S5) showed that these materials also exhibited a microporous character and excellent thermal stability. The adsorption capacities at 25.0 °C and 1.0 bar were found to be 12.7 ± 0.3, 12.4 ± 0.3, and 10.4 ± 0.3 mmol g^{-1} for MIL-160, CAU-10-pydc, and Al-Fum, respectively (Figure 6). PXRD and SEM results (Figures S20 and S24−S26) indicate that these MOFs are also stable after NH_3 adsorption, and the microporous character was kept unchanged (Figure S23 and Table S6). Moreover, the adsorption capacities at the lowest-pressure point on the desorption curves of MIL-160, CAU-10-pydc, and Al-Fum were 8.9, 6.6, and 3.2 mmol g^{-1} (Figure 6), corresponding to 1.76, 1.38, and 0.50 molecules of NH_3 per framework unit, respectively. The unit NH_3 uptake capacities of MIL-160 and CAU-10-pydc were about 3.5 and 2.8 times that of Al-Fum. Compared with the adsorption capacity of MOF-303(Al), this result indicates that the number of the sites on the MOFs significantly affected the NH_3 adsorption capacity of MOF, and the more the hydrogen bonding interaction sites, the higher the adsorption capacity. Therefore, our philosophy of multiple adsorption site ligands is an efficient and a successful strategy for high and reversible NH_3 uptake by MOFs.

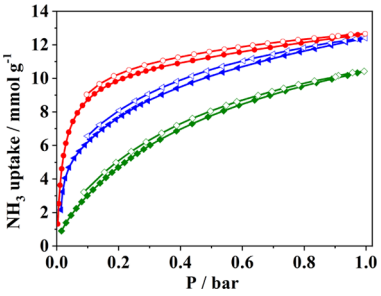

Figure 6. Adsorption isotherms of NH_3 on MIL-160, CAU-10-pydc, and Al-Fum at 25.0 °C and 1.0 bar: red circle, MIL-160; blue triangle, CAU-10-pydc; green diamond, Al-Fum; solid symbols, adsorption; open symbols, desorption.

CONCLUSIONS

In summary, we demonstrated a multiple hydrogen bonding interaction strategy for highly efficient and reversible NH_3 capture by increasing the active site number in ligands and selecting a relative inert metal node in MOFs. Under the guidance of this strategy, MOF-303(Al) synthesized in this work exhibited a high NH_3 adsorption capacity (19.7 mmol g^{-1} at 25.0 °C and 1.0 bar) and an outstanding reversibility (at least 20 cycles). Importantly, MOF-303(Al) could efficiently capture NH_3 at high temperatures or ultralow pressures, which provides the possibility for the removal and storage of trace NH_3 contaminant from polluted air and of real industrial waste gas. It is revealed that the superior NH_3 capacity and excellent reversibility of MOF-303(Al) resulted from the hydrogen bonding interactions of NH_3 with multiple adsorption sites of N−H, μ-OH, H−C, and N−N in MOF-303(Al), although the hydrogen bonding interactions of NH_3 with N−H and μ-OH adsorption sites were predominant. The molecular screening approach reported here exhibited the advantages of simplicity and high efficiency and might be used to design and screen MOF ligands quickly for efficient and reversible ammonia capture. This work opens a new pathway for the design and development of novel MOF adsorbents for the highly efficient capture and recovery of NH_3.

METHODS

Materials and the synthesis and characterization of the MOFs are given in the Supporting Information.

NH_3 Adsorption Experiments. NH_3 adsorption isotherms were determined by a BeiShiDe 3H-2000PM specific surface pore size analyzer at 25.0 °C. Before each adsorption experiment, 50−60 mg of the sample was weighed and degassed for 24 h at 150 °C under vacuum (<10^{-5} Pa). All ammonia analyses were performed in a Dewar flask. The MOFs were regenerated at 150 °C for 2 h under vacuum. CO_2 adsorption isotherms were determined by a BSD-PM2 surface pore size analyzer using a similar procedure. To confirm the reliability of the NH_3 adsorption data by this equipment, MIL-101(Cr) was synthesized and its surface area and pore volume were determined by a Quantachrome AUTOSORB-1 volumetric gas adsorption analyzer. The surface area of 2727 m^2/g and the pore volume of 1.48 cm^3/g were very close to those previously reported.[36] Then, MIL-101(Cr) was used to adsorb NH_3, and the capacity was 10.1 ± 0.2 mmol/g at 25.0 °C and 1.0 bar by using BeiShiDe 3H-2000PM equipment, which was in good agreement with the reported data in the literature.[36]

Breakthrough Experiments. The breakthrough experiments were performed by a SIRIUS-XF-30 instrument. The contents of water and NH_3 were determined by a GC9790II gas chromatograph. For all of the breakthrough experiments, about 60−80 mg of MOF-303(Al) was activated at 150 °C under N_2 for 24 h in the absorption column (4 × 250 mm). Taking the experiment with 5000 ppm of ammonia as an example, 5000 ppm of ammonia balanced with dry N_2 passed through the absorption column at 25.0 °C. For the humid ammonia experiments (10, 20, 40, and 80% RH), MOF-303(Al) was presaturated under the corresponding humid N_2 gas for 2 h at 25.0 °C. Then, 5000 ppm of NH3 diluted with the humid N_2 passed through the absorption column at 25.0 °C. The flow rate of 20 mL/min of the mixed gas was used in all experiments. A similar procedure was adopted for the measurements of NH_3 at other concentrations and humidities.

Variable Temperature Mid-infrared Spectra of MOF-303(Al) after NH_3 Adsorption. Typically, 20 mg of material was kept at 150 °C under dynamic vacuum for 12 h and then cooled to room temperature. Next, the activated MOF was exposed to a dry NH_3 environment at 1.0 bar for 24 h at 25.0 °C. For variable temperature mid-IR spectrum measurements, MOF-303(Al) after NH_3 adsorption was heated from 25 °C to 150 °C with a temperature interval of at least 10 °C, the sample was standing at each studied temperature for 20 min before further heating, and the IR spectra were recorded at different temperatures.

Far-IR Spectra of MOF-303(Al) before and after NH_3 Adsorption. Far-IR spectrum measurements were completed according to the procedure described in the literature.[62] For this purpose, a PE 400 far-IR spectrometer was used, which was composed of a room-temperature DTGS detector with a preamplifier and polyethylene (PE) windows with a 5 mm internal optical path. The wavenumber range was from 50 to 200 cm^{-1}, and the resolution of the far-IR spectrometer was 2 cm^{-1}. In the experiments, a small amount of MOF-303(Al) was mixed with PE to prepare a transparent sheet, and each far-IR spectrum was the result of 200 signal averaged scans.

DFT Calculations. All density functional theory calculations were performed by the Gaussian 16 program.[63] Molecular electrostatic potentials (MEPs) were evaluated at the B3LYP/6-311++G(d,p) level of theory. The hybrid exchange-correlation functional B3LYP was employed to optimize all structures of the ground states. For H, C, N, and O atoms, the basis set 6-311+g(d,p) was adopted here. For the metal atom Al, the effective pseudopotential double-ζ (LANL2DZ) basis set was used. Vibrational frequency calculations showed that all the optimized structures were minima on the potential energy surfaces of electronic ground states. All energies were corrected by considering

https://doi.org/10.1021/acsami.1c14470
ACS Appl. Mater. Interfaces 2021, 13, 56025−56034

zero-point energies and enthalpies at 25.0 °C and 1.0 bar. The hydrogen bonding interaction energies of NH_3 with MOF-303(Al) were estimated by the following equation:

$$E_{ads} = E_{H_3N\cdots H(MOF-303(A1))} - E_{MOF-303(A1)} - E_{NH_3} \quad (1)$$

where $E_{H_3N\cdots H(MOF-303(A1))}$, $E_{MOF-303(A1)}$, and E_{NH_3} are the hydrogen bonding interaction energies of NH_3 with MOF-303(Al) and Gibbs free energies of neat MOF-303(Al) and free NH_3 molecule, respectively.

■ ASSOCIATED CONTENT

Supporting Information

The Supporting Information is available free of charge at https://pubs.acs.org/doi/10.1021/acsami.1c14470.

Additional experimental details; tables containing the physicochemical property of the MOFs; figures including the chemical structure of the possible ligands, framework structures, SEM images, FT-IR spectra, XRD patterns, TGA curves, N_2 adsorption isotherms, XPS spectra of MOFs, and adsorption configurations of NH_3 on the sites of MOF-303(Al) (PDF)

■ AUTHOR INFORMATION

Corresponding Authors

Zhiyong Li − *Henan Key Laboratory of Green Chemistry, Collaborative Innovation Center of Henan Province for Green Manufacturing of Fine Chemicals, Key Laboratory of Green Chemical Media and Reactions, Ministry of Education, School of Chemistry and Chemical Engineering, Henan Normal University, Xinxiang, Henan 453007, P. R. China*; Email: yli@htu.edu.cn

Jianji Wang − *Henan Key Laboratory of Green Chemistry, Collaborative Innovation Center of Henan Province for Green Manufacturing of Fine Chemicals, Key Laboratory of Green Chemical Media and Reactions, Ministry of Education, School of Chemistry and Chemical Engineering, Henan Normal University, Xinxiang, Henan 453007, P. R. China*; orcid.org/0000-0003-2417-4630; Email: jwang@htu.edu.cn

Authors

Zhenzhen Wang − *Henan Key Laboratory of Green Chemistry, Collaborative Innovation Center of Henan Province for Green Manufacturing of Fine Chemicals, Key Laboratory of Green Chemical Media and Reactions, Ministry of Education, School of Chemistry and Chemical Engineering, Henan Normal University, Xinxiang, Henan 453007, P. R. China*

Xia-Guang Zhang − *Henan Key Laboratory of Green Chemistry, Collaborative Innovation Center of Henan Province for Green Manufacturing of Fine Chemicals, Key Laboratory of Green Chemical Media and Reactions, Ministry of Education, School of Chemistry and Chemical Engineering, Henan Normal University, Xinxiang, Henan 453007, P. R. China*; orcid.org/0000-0002-9223-0852

Qingchun Xia − *Henan Key Laboratory of Green Chemistry, Collaborative Innovation Center of Henan Province for Green Manufacturing of Fine Chemicals, Key Laboratory of Green Chemical Media and Reactions, Ministry of Education, School of Chemistry and Chemical Engineering, Henan Normal University, Xinxiang, Henan 453007, P. R. China*; orcid.org/0000-0002-4367-9194

Huiyong Wang − *Henan Key Laboratory of Green Chemistry, Collaborative Innovation Center of Henan Province for Green Manufacturing of Fine Chemicals, Key Laboratory of Green Chemical Media and Reactions, Ministry of Education, School of Chemistry and Chemical Engineering, Henan Normal University, Xinxiang, Henan 453007, P. R. China*

Chenlu Wang − *Beijing Key Laboratory of Ionic Liquids Clean Process, Institute of Process Engineering, Chinese Academy of Sciences, Beijing 100190, P. R. China*

Yanlei Wang − *Beijing Key Laboratory of Ionic Liquids Clean Process, Institute of Process Engineering, Chinese Academy of Sciences, Beijing 100190, P. R. China*; orcid.org/0000-0002-2214-8781

Hongyan He − *Beijing Key Laboratory of Ionic Liquids Clean Process, Institute of Process Engineering, Chinese Academy of Sciences, Beijing 100190, P. R. China*; orcid.org/0000-0003-1291-2771

Yang Zhao − *Henan Key Laboratory of Green Chemistry, Collaborative Innovation Center of Henan Province for Green Manufacturing of Fine Chemicals, Key Laboratory of Green Chemical Media and Reactions, Ministry of Education, School of Chemistry and Chemical Engineering, Henan Normal University, Xinxiang, Henan 453007, P. R. China*

Complete contact information is available at: https://pubs.acs.org/10.1021/acsami.1c14470

Notes

The authors declare no competing financial interest.

■ ACKNOWLEDGMENTS

The authors gratefully acknowledge the financial support from the National Natural Science Foundation of China (nos. U1704251, 21733011, and 21801068), the National Key Research and Development Program of China (no. 2017YFA0403101), Program for Universities of Henan Province Science & Technology Innovation Talents (no. 21HASTIT003), and the 111 project (no. D17007).

■ REFERENCES

(1) Schüth, F.; Palkovits, R.; Schlögl, R.; Su, D. S. Ammonia as a Possible Element in an Energy Infrastructure: Catalysts for Ammonia Decomposition. *Energy Environ. Sci.* **2012**, *5*, 6278−6289.

(2) DeCoste, J. B.; Denny, J. M. S.; Peterson, G. W.; Mahle, J. J.; Cohen, S. M. Enhanced Aging Properties of HKUST-1 in Hydrophobic Mixed-Matrix Membranes for Ammonia Adsorption. *Chem. Sci.* **2016**, *7*, 2711−2716.

(3) Faulkner, W. B.; Shaw, B. W. Review of Ammonia Emission Factors for United States Animal Agriculture. *Atmos. Environ.* **2008**, *42*, 6567−6574.

(4) Palomar, J.; Gonzalez-Miquel, M.; Bedia, J.; Rodriguez, F.; Rodriguez, J. J. Task-specific Ionic Liquids for Efficient Ammonia Absorption. *Sep. Purif. Technol.* **2011**, *82*, 43−52.

(5) Warner, J. X.; Dickerson, R. R.; Wei, Z.; Strow, L. L.; Wang, Y.; Liang, Q. Increased Atmospheric Ammonia over the World's Major Agricultural Areas Detected from Space. *Geophys. Res. Lett.* **2017**, *44*, 2875−2884.

(6) Erisman, J. W.; Bleeker, A.; Galloway, J.; Sutton, M. S. Reduced Nitrogen in Ecology and the Environment. *Environ. Pollut.* **2007**, *150*, 140−149.

(7) Rieth, A. J.; Dincă, M. Programming Framework Materials for Ammonia Capture. *ACS Cent. Sci.* **2018**, *4*, 666−667.

(8) Helminen, J.; Helenius, J.; Paatero, E.; Turunen, I. Adsorption Equilibria of Ammonia Gas on Inorganic and Organic Sorbents at 298. 15 K. *J. Chem. Eng. Data* **2001**, *46*, 391−399.

(9) Qajar, A.; Peer, M.; Andalibi, M. R.; Rajagopalan, R.; Foley, H. C. Enhanced Ammonia Adsorption on Functionalized Nanoporous Carbons. *Microporous Mesoporous Mater.* **2015**, *218*, 15−23.
(10) Tamainot-Telto, Z.; Metcalf, S. J.; Critoph, R. E.; Zhong, Y.; Thorpe, R. Carbon−Ammonia Pairs for Adsorption Refrigeration Applications: Ice Making, Air Conditioning and Heat Pumping. *Int. J. Refrig.* **2009**, *32*, 1212−1229.
(11) Van Humbeck, J. F.; McDonald, T. M.; Jing, X.; Wiers, B. M.; Zhu, G.; Long, J. R. Ammonia Capture in Porous Organic Polymers Densely Functionalized with Brønsted Acid Groups. *J. Am. Chem. Soc.* **2014**, *136*, 2432−2440.
(12) Molina-Sabio, M.; González, J. C.; Rodríguez-Reinoso, F. Adsorption of NH3 and H2S on Activated Carbon and activated Carbon-Sepiolite Pellets. *Carbon* **2004**, *42*, 448−450.
(13) Wang, H.; Song, T.; Li, Z.; Qiu, J.; Zhao, Y.; Zhang, H.; Wang, J. Exceptional High and Reversible Ammonia Uptake by Two Dimension Few-Layer BiI_3 nanosheets. *ACS Appl. Mater. Interfaces* **2021**, *13*, 25918−25925.
(14) Rieth, A. J.; Wright, A. M.; Dincă, M. Kinetic Stability of Metal−Organic Frameworks for Corrosive and Coordinating Gas Capture. *Nat. Rev. Mater.* **2019**, *4*, 708−725.
(15) Sumida, K.; Rogow, D. L.; Mason, J. A.; McDonald, T. M.; Bloch, E. D.; Herm, Z. R.; Bae, T.-H.; Long, J. R. Carbon Dioxide Capture in Metal-Organic Frameworks. *Chem. Rev.* **2012**, *112*, 724−781.
(16) Li, J.-R.; Ma, Y.; McCarthy, M. C.; Sculley, J.; Yu, J.; Jeong, H.-K.; Balbuena, P. B.; Zhou, H.-C. Carbon Dioxide Capture-Related Gas Adsorption and Separation in Metal-Organic Frameworks. *Coord. Chem. Rev.* **2011**, *255*, 1791−1823.
(17) Britt, D.; Tranchemontagne, D.; Yaghi, O. M. Metal-Organic Frameworks with High Capacity and Selectivity for Harmful Gases. *Proc. Natl. Acad. Sci. U. S. A.* **2008**, *105*, 11623−11627.
(18) Liu, L.; Wang, L.; Liu, D.; Yang, Q.; Zhong, C. High-Throughput Computational Screening of Cu-MOFs with Open Metal Sites for Efficient C_2H_2/C_2H_4 Separation. *Green Energy Environ.* **2020**, *5*, 333−340.
(19) Furukawa, H.; Cordova, K. E.; O'Keeffe, M.; Yaghi, O. M. The Chemistry and Applications of Metal-Organic Frameworks. *Science* **2013**, *341*, 123004.
(20) Vikrant, K.; Kumar, V.; Kim, K.-H.; Kukkar, D. Metal-Organic Frameworks (Mofs): Potential and Challenges for Capture and Abatement of Ammonia. *J. Mater. Chem. A* **2017**, *5*, 22877−22896.
(21) Bobbitt, N. S.; Mendonca, M. L.; Howarth, A. J.; Islamoglu, T.; Hupp, J. T.; Farha, O. K.; Snurr, R. Q. Metal-Organic Frameworks for the Removal of Toxic Industrial Chemicals and Chemical Warfare Agents. *Chem. Soc. Rev.* **2017**, *46*, 3357−3385.
(22) Qiao, C.; Lu, L.; Xu, W.; Xia, Z.; Zhou, C.; Chen, S.; Gao, S. Synthesis, Thermal Decomposition Kinetics and Detonation Performance of a Three-Dimensional Solvent-Free Energetic Ag(I)-MOF. *Acta Phys.-Chim. Sin.* **2020**, *36*, 1905085.
(23) Saha, D.; Deng, S. Ammonia Adsorption and its Effects on framework Stability of MOF-5 and MOF-177. *J. Colloid Interface Sci.* **2010**, *348*, 615−620.
(24) Katz, M. J.; Howarth, A. J.; Moghadam, P. Z.; DeCoste, J. B.; Snurr, R. Q.; Hupp, J. T.; Farha, O. K. High Volumetric Uptake of Ammonia Using Cu-MOF-74/Cu-CPO-27. *Dalton Trans.* **2016**, *45*, 4150−4153.
(25) Peterson, G. W.; Wagner, G. W.; Balboa, A.; Mahle, J.; Sewell, T.; Karwacki, C. J. Ammonia Vapor Removal by $Cu_3(BTC)_2$ and its Characterization by MAS NMR. *J. Phys. Chem. C* **2009**, *113*, 13906−13917.
(26) Rieth, A. J.; Dincă, M. Controlled Gas Uptake in Metal-Organic Frameworks with Record Ammonia Sorption. *J. Am. Chem. Soc.* **2018**, *140*, 3461−3466.
(27) Rieth, A. J.; Tulchinsky, Y.; Dincă, M. High and Reversible Ammonia Uptake in Mesoporous Azolate Metal Organic Frameworks with Open Mn, Co, and Ni Sites. *J. Am. Chem. Soc.* **2016**, *138*, 9401−9404.
(28) Chen, Y.; Du, Y.; Liu, P.; Yang, J.; Li, L.; Li, J. Removal of Ammonia Emissions via Reversible Structural Transformation in M(BDC) (M = Cu, Zn, Cd) Metal−Organic Frameworks. *Environ. Sci. Technol.* **2020**, *54*, 3636−3642.
(29) Nguyen, T. N.; Harreschou, I. M.; Lee, J. H.; Stylianou, K. C.; Stephan, D. W. A Recyclable Metal-Organic Framework for Ammonia Vapour Adsorption. *Chem. Commun.* **2020**, *56*, 9600−9603.
(30) Godfrey, H. G. W.; da Silva, I.; Briggs, L.; Carter, J. H.; Morris, C. G.; Savage, M.; Easun, T. L.; Manuel, P.; Murray, C. A.; Tang, C. C.; Frogley, M. D.; Cinque, G.; Yang, S.; Schroëer, M. Ammonia Storage by Reversible Host-Guest Site Exchange in a Robust Metal-Organic Framework. *Angew. Chem., Int. Ed.* **2018**, *57*, 14778−14781.
(31) Jasuja, H.; Peterson, G. W.; Decoste, J. B.; Browe, M. A.; Walton, K. S. Evaluation of MOFs for Air Purification and Air Quality Control Applications: Ammonia Removal from Air. *Chem. Eng. Sci.* **2015**, *124*, 118−124.
(32) Zhang, Y.; Zhang, X.; Chen, Z.; Otake, K.-i.; Peterson, G. W.; Chen, Y.; Wang, X.; Redfern, L. R.; Goswami, S.; Li, P.; Islamoglu, T.; Wang, B.; Farha, O. K. A Flexible Interpenetrated Zirconium-based Metal−Organic Framework with High Affinity Toward Ammonia. *ChemSusChem* **2020**, *13*, 1710−1714.
(33) Liu, J.; Chen, Z.; Wang, R.; Alayoglu, S.; Islamoglu, T.; Lee, S.-J.; Sheridan, T. R.; Chen, H.; Snurr, R. Q.; Farha, O. K.; Hupp, J. T. Zirconium Metal−Organic Frameworks Integrating Chloride Ions for Ammonia Capture and/or Chemical Separation. *ACS Appl. Mater. Interfaces* **2021**, *13*, 22485−22494.
(34) Marsh, C.; Han, X.; Li, J.; Lu, Z.; Argent, S. P.; da Silva, I.; Cheng, Y.; Daemen, L. L.; Ramirez-Cuesta, A. J.; Thompson, S. P.; Blake, A. J.; Yang, S.; Schröder, M. Exceptional Packing Density of Ammonia in a Dual-Functionalized Metal−Organic Framework. *J. Am. Chem. Soc.* **2021**, *143*, 6586−6592.
(35) Chen, Y.; Zhang, X.; Ma, K.; Chen, Z.; Wang, X.; Knapp, J.; Alayoglu, S.; Wang, F.; Xia, Q.; Li, Z.; Islamoglu, T.; Farha, O. K. Zirconium-based Metal-Organic Framework with 9-Connected Nodes for Ammonia Capture. *ACS Appl. Nano Mater.* **2019**, *2*, 6098−6102.
(36) Chen, Y.; Zhang, F.; Wang, Y.; Yang, C.; Yang, J.; Li, J. Recyclable Ammonia Uptake of a MIL Series of Metal-Organic Frameworks with High Structural Stability. *Microporous and Mesoporous Mater.* **2018**, *258*, 170−177.
(37) Han, X.; Lu, W.; Chen, Y.; da Silva, I.; Li, J.; Lin, L.; Li, W.; Sheveleva, A. M.; Godfrey, H. G. W.; Lu, Z.; Tuna, F.; McInnes, E. J. L.; Cheng, Y.; Daemen, L. L.; McPherson, L. J. M.; Teat, S. J.; Frogley, M. D.; Rudić, S.; Manuel, P.; Ramirez-Cuesta, A. J.; Yang, S.; Schröder, M. High Ammonia Adsorption in MFM-300 Materials: Dynamics and Charge Transfer in Host−Guest Binding. *J. Am. Chem. Soc.* **2021**, *143*, 3153−3161.
(38) Kim, D. W.; Kang, D. W.; Kang, M.; Lee, J.-H.; Choe, J. H.; Chae, Y. S.; Choi, D. S.; Yun, H.; Hong, C. S. High Ammonia Uptake of a Metal−Organic Framework Adsorbent in a Wide Pressure Range. *Angew. Chem., Int. Ed.* **2020**, *59*, 22531−22536.
(39) Demessence, A.; D'Alessandro, D. M.; Foo, M. L.; Long, J. R. Strong CO_2 Binding in a Water-Stable, Triazolate-Bridged Metal−Organic Framework Functionalized with Ethylenediamine. *J. Am. Chem. Soc.* **2009**, *131*, 8784−8786.
(40) Bae, Y.-S.; Snurr, R. Q. Development and Evaluation of Porous Materials for Carbon Dioxide Separation and Capture. *Angew. Chem., Int. Ed.* **2011**, *50*, 11586−11596.
(41) Wang, B.; Huang, H.; Lv, X.-L.; Xie, Y.; Li, M.; Li, J.-R. Tuning CO_2 Selective Adsorption over N_2 and CH_4 in UiO-67 Analogues through Ligand Functionalization. *Inorg. Chem.* **2014**, *53*, 9254−9259.
(42) Bobinihi, F. F.; Onwudiwe, D. C.; Ekennia, A. C.; Okpareke, O. C.; Arderne, C.; Lane, J. R. Group 10 Metal Complexes of Dithiocarbamates Derived from Primary Anilines: Synthesis, Characterization, Computational and Antimicrobial Studies. *Polyhedron* **2019**, *158*, 296−310.
(43) Bulat, F. A.; Toro-Labbé, A.; Brinck, T.; Murray, J. S.; Politzer, P. Quantitative Analysis of Molecular Surfaces: Areas, Volumes, Electrostatic Potentials and Average Local Ionization Energies. *J. Mol. Model.* **2010**, *16*, 1679−1691.

https://doi.org/10.1021/acsami.1c14470
ACS Appl. Mater. Interfaces 2021, 13, 56025−56034

(44) Emsley, J. Very Strong Hydrogen Bonding. *Chem. Soc. Rev.* **1980**, *9*, 91−124.
(45) Fathieh, F.; Kalmutzki, M. J.; Kapustin, E. A.; Waller, P. J.; Yang, J. J.; Yaghi, O. M. Practical Water Production from Desert Air. *Sci. Adv.* **2018**, *4*, No. eaat3198.
(46) Wahiduzzaman, M.; Lenzen, D.; Maurin, G.; Stock, N.; Wharmby, M. T. Rietveld Refinement of MIL-160 and its Structural Flexibility upon H_2O and N_2 Adsorption. *Eur. J. Inorg. Chem.* **2018**, *2018*, 3626−3632.
(47) Wang, Y.; Zhao, X.; Yang, H.; Bu, X.; Wang, Y.; Jia, X.; Li, J.; Feng, P. A Tale of Two Trimers from Two Different Worlds: A COF-Inspired Synthetic Strategy for Pore-Space Partitioning of MOFs. *Angew. Chem., Int. Ed.* **2019**, *58*, 6316−6320.
(48) Dou, B.; Zhang, M.; Gao, J.; Shen, W.; Sha, X. High-Temperature Removal of NH_3, Organic Sulfur, HCl, and Tar Component from Coal-Derived Gas. *Ind. Eng. Chem. Res.* **2002**, *41*, 4195−4200.
(49) Thommes, M.; Kaneko, K.; Neimark, A. V.; Olivier, J. P.; Rodriguez-Reinoso, F.; Rouquerol, J.; Sing, K. S. W. Physisorption of Gases, with Special Reference to the Evaluation of Surface Area and Pore Size Distribution (IUPAC Technical Report). *Pure Appl. Chem.* **2015**, *87*, 1051−1069.
(50) Alvarez, E.; Guillou, N.; Martineau, C.; Bueken, B.; Van de Voorde, B.; Le Guillouzer, C.; Fabry, P.; Nouar, F.; Taulelle, F.; de Vos, D.; Chang, J.-S.; Cho, K. H.; Ramsahye, N.; Devic, T.; Daturi, M.; Maurin, G.; Serre, C. The Structure of the Aluminum Fumarate Metal-Organic Framework A520. *Angew. Chem., Int. Ed.* **2015**, *54*, 3664−3668.
(51) Doonan, C. J.; Tranchemontagne, D. J.; Glover, T. G.; Hunt, J. R.; Yaghi, O. M. Exceptional Ammonia Uptake by a Covalent Organic Framework. *Nat. Chem.* **2010**, *2*, 235−238.
(52) Permyakova, A.; Skrylnyk, O.; Courbon, E.; Affram, M.; Wang, S.; Lee, U. H.; Valekar, A. H.; Nouar, F.; Mouchaham, G.; Devic, T.; De Weireld, G.; Chang, J.-S.; Steunou, N.; Frere, M.; Serre, C. Synthesis Optimization, Shaping, and Heat Reallocation Evaluation of the Hydrophilic Metal-Organic Framework MIL-160(Al). *ChemSusChem* **2017**, *10*, 1419−1426.
(53) Shang, D.; Zhang, X.; Zeng, S.; Jiang, K.; Gao, H.; Dong, H.; Yang, Q.; Zhang, S. Protic Ionic Liquid $BimNTf_2$ with Strong Hydrogen Bond Donating Ability for Highly Efficient Ammonia Absorption. *Green Chem.* **2017**, *19*, 937−945.
(54) Kostova, I.; Peica, N.; Kiefer, W. Raman, FT-IR, and DFT Studies Of 3,5-Pyrazoledicarboxylic Acid and its Ce(III) and Nd(III) Complexes. *J. Raman Spectrosc.* **2007**, *38*, 1−10.
(55) Wharmby, M. T.; Snoyek, M.; Rhauderwiek, T.; Ritter, K.; Stock, N. Group 13 Metal Carboxylates: Using Molecular Clusters as Hybrid Building Units in a MIL-53 Type Framework. *Cryst. Growth Des.* **2014**, *14*, 5310−5317.
(56) Senkovska, I.; Hoffmann, F.; Fröba, M.; Getzschmann, J.; Böhlmann, W.; Kaskel, S. New Highly Porous Aluminium based Metal-Organic Frameworks: Al(OH)(ndc) (ndc=2,6-Naphthalene Dicarboxylate) and Al(OH)(bpdc) (bpdc=4,4′-Biphenyl Dicarboxylate). *Microporous and Mesoporous Mater.* **2009**, *122*, 93−98.
(57) Escamilla-Roa, E.; Sainz-Díaz, C. I. Effect of Amorphous Ammonia−Water Ice onto Adsorption of Glycine on Cometary Dust Grain and IR Spectroscopy. *J. Phys. Chem. C* **2014**, *118*, 26080−26090.
(58) Wulf, A.; Fumino, K.; Ludwig, R. Spectroscopic Evidence for an enhanced Anion−Cation Interaction from Hydrogen Bonding in Pure Imidazolium Ionic Liquids. *Angew. Chem., Int. Ed.* **2010**, *49*, 449−453.
(59) Yang, Y.; Faheem, M.; Wang, L.; Meng, Q.; Sha, H.; Yang, N.; Yuan, Y.; Zhu, G. Surface Pore Engineering of Covalent Organic Frameworks for Ammonia Capture Through Synergistic Multivariate and Open Metal Site Approaches. *ACS Cent. Sci.* **2018**, *4*, 748−754.
(60) Shallenberger, J. R.; Cole, D. A.; Novak, S. W. Characterization of Silicon Oxynitride Thin Films by X-Ray Photoelectron Spectroscopy. *J. Vac. Sci. Technol., A* **1999**, *17*, 1086−1090.
(61) Cadiau, A.; Lee, J. S.; Borges, D. D.; Fabry, P.; Devic, T.; Wharmby, M. T.; Martineau, C.; Foucher, D.; Taulelle, F.; Jun, C.-H.; Hwang, Y. K.; Stock, N.; De Lange, M. F.; Kapteijn, F.; Gascon, J.; Maurin, G.; Chang, J.-S.; Serre, C. Design of Hydrophilic Metal Organic Framework Water Adsorbents for Heat Reallocation. *Adv. Mater.* **2015**, *27*, 4775−4780.
(62) Zhang, Y.; Li, Z.; Wang, H.; Xuan, X.; Wang, J. Efficient Separation of Phenolic Compounds from Model Oil by the Formation of Choline Derivative-based Deep Eutectic Solvents. *Sep. Purif. Technol.* **2016**, *163*, 310−318.
(63) Frisch, M. J. T. G. W.; Schlegel, H. B.; Scuseria, G. E.; Robb, M. A.; Cheeseman, J. R.; Scalmani, G.; Barone, V.; Petersson, G. A.; Nakatsuji, H.; Li, X.; Caricato, M.; Marenich, A. V.; Bloino, J.; Janesko, B. G.; Gomperts, R.; Mennucci, B.; Hratchian, H. P.; Ortiz, J. V.; Izmaylov, A. F.; Sonnenberg, J. L.; Williams-Young, D.; Ding, F.; Lipparini, F.; Egidi, F.; Goings, J.; Peng, B.; Petrone, A.; Henderson, T.; Ranasinghe, D.; Zakrzewski, V. G.; Gao, J.; Rega, N.; Zheng, G.; Liang, W.; Hada, M.; Ehara, M.; Toyota, K.; Fukuda, R.; Hasegawa, J.; Ishida, M.; Nakajima, T.; Honda, Y.; Kitao, O.; Nakai, H.; Vreven, T.; Throssell, K.; Montgomery, J. A., Jr.; Peralta, J. E.; Ogliaro, F.; Bearpark, M. J.; Heyd, J. J.; Brothers, E. N.; Kudin, K. N.; Staroverov, V. N.; Keith, T. A.; Kobayashi, R.; Normand, J.; Raghavachari, K.; Rendell, A. P.; Burant, J. C.; Iyengar, S. S.; Tomasi, J.; Cossi, M.; Millam, J. M.; Klene, M.; Adamo, C.; Cammi, R.; Ochterski, J. W.; Martin, R. L.; Morokuma, K.; Farkas, O.; Foresman, J. B.; Fox, D. J., *Gaussian 16 Revision B01*; Gaussian, Inc.: Wallingford, CT, 2016.

https://doi.org/10.1021/acsami.1c14470
ACS Appl. Mater. Interfaces 2021, 13, 56025−56034